08,04

# Paramagnetic centers of vanadium and iron in $Na_5AlF_2(PO_4)_2$ single crystal

© V.A. Vazhenin, A.V. Fokin, A.P. Potapov, M.Yu. Artyomov

Ural Federal University, Institute of Natural Sciences and Mathematics,
Russia, Yekaterinburg

E-mail: Vladimir.Vazhenin@urfu.ru

*Received November 18, 2022*
*Revised November 18, 2022*
*Accepted November 25, 2022*

The orientation behavior of the EPR-transitions of uncontrolled $V^{4+}$ ($S = 1/2$) and $Fe^{3+}$ ($S = 5/2$) impurity centers in a $Na_5AlF_2(PO_4)_2$ single crystal doped with chromium has been studied. The parameters of the spin Hamiltonian of these centers are determined both in the laboratory (crystallographic) and in the local coordinate systems. Based on the fact of the existence of mixed vanadate-phosphates and taking into account the orientation of the principal axis $V^{4+}$, it was concluded that vanadium replaced the position of phosphorus. The closeness of the principal axes of the fine structure tensors of the second and fourth ranks of $Fe^{3+}$ centers to the F-F direction of the fluorine-oxygen octahedron surrounding the iron ion was found.

**Keywords:** impurity ions, paramagnetic resonance, hyperfine interaction.

DOI: 10.21883/PSS.2023.02.55416.530

## 1. Introduction

In Ref. [1] reported the investigation of the electron paramagnetic resonance (EPR) of Chromium-doped $Na_5AlF_2(PO_4)_2$ (NAPF) single crystal. The authors found intensive spectra of trivalent chromium ions, vanadium ion transitions and non-identified center signals. Fine structure parameters of $Cr^{3+}$ ions which replaced $Al^{3+}$ ions in triclinic positions were initially detected in the coordinate system whose axes are associated with crystallographic axes. In the found local coordinate system, the spectra of these centers are described by the spin Hamiltonian (SH) of rhombic symmetry.

Authors of [2–5] have earlier investigated crystalline structure and ion conductivity (due to sodium ion transfer) in $Na_5AlF_2(PO_4)_2$ and $Na_5GaF_2(PO_4)_2$. In both crystals, structural transition at $\sim 545$ K was detected. The ionic conductivity of these compounds ($\sim 10^{-7}$ S/cm at 293 K) increases with temperature and achieves $\sim 10^{-4}$ S/cm at 600 K [4]. Structural data given in [2,3] is very similar, but the $z$-coordinates of atoms have different signs. Springer Materials base refers to [2] and we use this structural data.

EPR spectrum orientation dependences of NAPF crystal are investigated herein in order to identify vanadium SH center parameters and to describe impurity centers that have not been identified earlier in [1], both in crystallographic and local coordinate systems.

## 2. Samples and measurement procedure

$Na_5AlF_2(PO_4)_2$ single crystals were grown at Shubnikov Institute of Crystallography of the Russian Academy of Sciences by solution-melt crystallization [6] at $\sim 1000$ K.

$Na_5AlF_2(PO_4)_2$ space group at room temperature is $P\bar{3}(C_{3i}^1)$, the lattice parameters are: $a = b = 10.483(1)$ Å, $c = 6.607(1)$ Å [2], $a = b = 10.468(3)$ Å, $c = 6.599(2)$ Å [3]. The crystal structure contains six independent positions of sodium ions with a coordination number of 6 and point symmetry groups $\bar{3}(C_{3i})$ {Na1, Na3}, 3 ($C_3$) {$Na_5$, $Na_6$}, $\bar{1}$ ($C_i$) {Na2} and 1 ($C_1$) {Na4} [2–3]. The environment of various sodium ions is either pure oxygen {Na1, Na3} or mixed — fluorine-oxygen. The spacing between sodium and fluorine in the latter is 2.33–2.45 Å. Aluminum ions in this crystal have one position with $\bar{1}$ ($C_i$) symmetry and are surrounded by four oxygen ions and two fluorine ions with the octahedron compressed in the fluorine-fluorine direction ($R = 1.83$ Å instead of 1.87–1.9 Å) [2–3]. Phosphorus also has only one position in the oxygen tetrahedron, but with local 1 ($C_1$) symmetry and phosphorus-oxygen spacing in $PO_4$ 1.522–1.549 Å tetrahedra typical of orthophosphates [2]. It is natural that all triclinic positions are multiplied up to three by $C_3$ crystal symmetry operation.

Measurements were performed at room temperature and 115 K using EMX Plus Bruker EPR X-band spectrometer. The specimens oriented in an X-ray diffractometer were secured in the spectrometer resonant cavity to a holder attached to the standard automatic goniometer rod and capable of rotating around the axis at right angle to the rod.

## 3. Experimental results and discussion

### 3.1. $V^{4+}$ centers

In [1], the observation in the NAPF near $g = 2$ (Figure 2) of an octet of narrow weak signals with a spread of 92 mT was reported. Such hyperfine structure is most likely

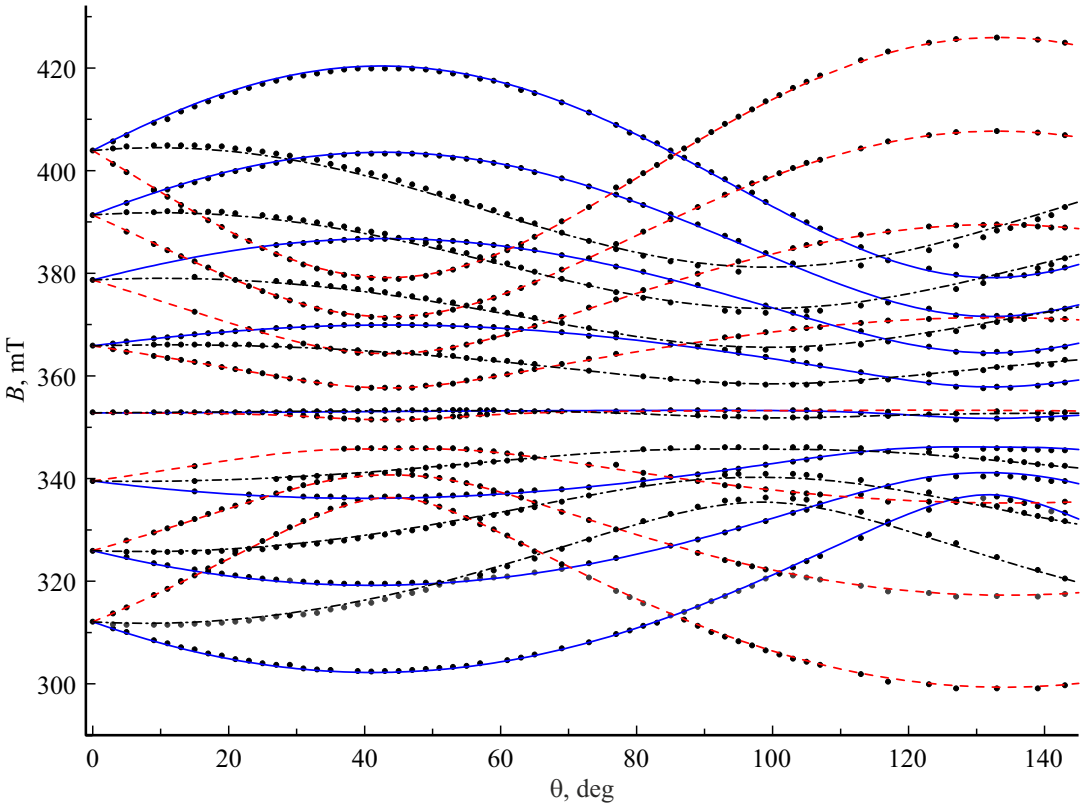


**Figure 1.** Polar angular dependence in the $ZX$ plane of positions of the hyperfine structure components of three $V^{4+}$ center transitions coupled by $C_3$ operation. Solid curves — $\varphi = 0°$, dashed curves — $\varphi = 120°$, dash-dotted black curves — $\varphi = 240°$.

caused by $^{51}V$ ion isotope having $I = 7/2$ nuclear spin and natural abundance of 99.76%. The aforesaid vanadium centers demonstrate the orientational behavior of the positions of eight hyperfine components of three equivalent but rotated centers in the $ZX$ plane, as shown in Figure 1. For this, the following rectangular laboratory coordinate system (CS) is used: $Z \parallel c \parallel C_3$ of the crystal and axis $Y$ is at $\Delta\varphi = +12.5°$ from the crystallographic $b$ axis. Since no other electronic transitions of vanadium centers with similar hyperfine structure were observed in the magnetic field range up to 1.5 T, it can be reasonably suggested that the observed typical polar dependence of the spectrum with nearly isotropic $g$-tensor is caused by $V^{4+}$ ions with electron spin $S = 1/2$ in $3d^1$ configuration. $V^{4+}$ centers with similar Zeeman and hyperfine interaction parameters were observed in [7–12] in $Al_2O_3$, $TiO_2$, $SnO_2$, $KTiOPO_4$, $NaTiOPO_4$ and $\alpha$-$RbTiOPO_4$ crystals.

Vanadium spectrum and orientation behavior were described by spin Hamiltonian

$$H_{sp} = \beta(\mathbf{BgS}) + \mathbf{SAI} + g_N\beta_N\mathbf{BI}, \qquad (1)$$

where $\mathbf{g}$ is the electron $\mathbf{g}$-tensor, $\mathbf{A}$ is the hyperfine interaction tensor, $\beta$ is the Bohr magneton, $\mathbf{B}$ is the magnetic field induction. The calculations used tabular values of vanadium nuclear $g_N$-factor ($\beta_N$ — nuclear magneton), nuclear quadrupole interaction was ignored because of its smallness [8].

As a result of rms deviation minimization of calculated and measured transition frequencies using 679 resonant positions and complex 16-th order energy matrix $\{(2 \cdot S + 1) \cdot (2 \cdot I + 1)\}$, $\mathbf{g}$- and $\mathbf{A}$-tensor elements where obtained (where $A_{ik}$ in MHz):

$$\mathbf{g} = \begin{vmatrix} 1.9499 & -0.0497 & -0.0236 \\ 0.0383 & 1.9536 & 0.0269 \\ 0.0034 & -0.0438 & 1.9509 \end{vmatrix},$$

$$\mathbf{A} = \begin{vmatrix} 228.7 & -36.3 & 244.5 \\ 21.1 & 116.4 & 244.8 \\ 23.4 & -124.0 & 338.9 \end{vmatrix}. \qquad (2)$$

Due to the low symmetry of the vanadium centers, only when all aforesaid $\mathbf{g}$ and $\mathbf{A}$ tensor elements were taken into account, the measured polar dependence (rms deviation = 4.6 MHz) was sufficiently well described, as shown in Figure 1.

As a result of $\mathbf{g}^2$ and $\mathbf{A}^2$ [13–14] tensor diagonalization, the following ($A_{ik}$ in MHz) parameters and direction cosine matrices, which put together the laboratory CS and principal axes system, were obtained

$$g_{xx} = 1.9358, \quad g_{yy} = 1.9584, \quad g_{zz} = 1.9619,$$

$$\begin{pmatrix} 0.6016 & -0.7183 & -0.3494 \\ 0.4863 & 0.6764 & -0.5532 \\ 0.6336 & 0.1629 & 0.7563 \end{pmatrix},$$

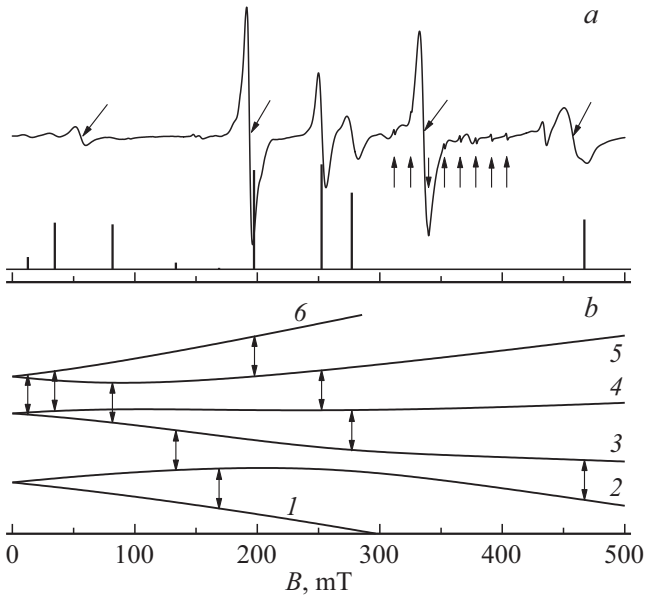


**Figure 2.** EPR spectrum (first derivative of the absorption signal) of chromium doped $Na_5AlF_2(PO_4)_2$ with $B \parallel C_3$ at 9844 MHz, as well as calculated positions and integral intensities of $Fe^{3+}$ center transitions. ($a$) inclined arrows indicate $Cr^{3+}$ signals, vertical arrows indicate $V^{4+}$ transitions, ($b$) energy levels (1–6) and $Fe^{3+}$ center transitions.

$$A_{xx} = 165.2, \quad A_{yy} = 174.5, \quad A_{zz} = 510.2,$$
$$\begin{pmatrix} 0.2924 & 0.7433 & 0.6016 \\ 0.6537 & -0.6145 & 0.4415 \\ -0.6979 & -0.2642 & 0.6657 \end{pmatrix}. \qquad (3)$$

Therefore, symmetry (pseudosymmetry) of $V^{4+}$ centers in NAPF may be assumed as approximately rhombic, but with various directions of the principal axes of $g$- and $A$-tensors. It should be noted that weak anisotropy of $g$-tensor can results in high errors in the cosine matrix elements.

Return to the laboratory system using the obtained diagonal **g**- and **A**-tensors and direction cosine matrices results in the following, definitely symmetrical, type of tensors

$$\mathbf{g} = \begin{vmatrix} 1.9506 & -0.0059 & -0.0096 \\ -0.0059 & 1.9541 & -0.0085 \\ 0.0096 & -0.0085 & 1.9514 \end{vmatrix},$$
$$\mathbf{A} = \begin{vmatrix} 295.2 & 87.4 & 136.3 \\ 87.4 & 236.0 & 102.9 \\ 136.3 & 102.9 & 318.7 \end{vmatrix}. \qquad (4)$$

These tensors describe the measured dependences with rms deviation 13.6 MHz. Optimization of only diagonal tensor elements decreases the specified deviation to 8.6 MHz with the following values obtained:

$$g_{xx} = 1.9507, \quad g_{yy} = 1.9541, \quad g_{zz} = 1.9514,$$
$$A_{xx} = 288.0, \quad A_{yy} = 247.4, \quad A_{zz} = 316.3\,MHz. \qquad (5)$$

Due to low symmetry of $V^{4+}$ centers in NAPF, **g**- and **A**-tensors probably contain antisymmetric contributions and, therefore, the used tensor symmetrization procedure causes some errors.

Positioning of $V^{4+}$ ion in NAPF structure was discussed in [1], potential substitution of aluminum and sodium positions was addressed. However, the vanadium ion is likely placed in the phosphorus atom position as indicated in [15], where the occurrence of mixed vanadate-phosphates in $MZr_2(VO_4)_x(PO_4)_{3-x}$ systems (where $M$ is an alkaline metal) is demonstrated. The frame of such compounds with kosnarite structure is built of tetrahedra statistically populated with vanadium and phosphorus atoms and $ZrO_6$-octahedra [15]. However, quinquivalent vanadium ion is addressed therein, but the anion vacancies existing in NAPF crystal may cause vanadium recharge. The absence of superhyperfine structure from fluorine (Figure 2 [1] at 1.4 mT signal width) at the vanadium centers also counts in favor of $V^{4+}$ ion placement in the phosphorus site, no superstructure is also observed at 115 K with 1.2 mT signal width. This is natural, because the distance to the nearest fluorine ions from phosphorus positions is $\sim 3.5$ Å and is much greater than from aluminum positions.

According to cosine matrix (3), the angle between the principal axes of $V^{4+}$ ion hyperfine interaction tensor in the laboratory and local coordinate systems is equal to $\sim 48°$, while the equivalent angle for **g**-tensor is $\sim 40°$. The direction from the phosphorus atom towards one of the oxygen tetrahedron vertices is spaced away from $Z \parallel c$ by $\sim 44°$. Taking into account the structural differences in phosphorus-oxygen distances (see Section 2) and angles between the directions towards the tetrahedron vertices ($105–112°$), the obtained mismatch may be considered as absolutely natural.

### 3.2. $Fe^{3+}$ centers

Figure 2 in [1] and Figure 2, $a$ herein show that, in addition to $Cr^{3+}$ and $V^{4+}$ ion spectra, other non-identified EPR signals are observed in NAPF. We managed to describe the signal group including the most strong transitions (Figure 2, $a$ herein) by the spin Hamiltonian of the triclinic symmetry [16] with electron spin $S = 5/2$:

$$H_{sp} = \beta(\mathbf{BgS}) + \frac{1}{3} \cdot \sum_m \left(b_{2m}O_{2m} + c_{2m}\Omega_{2m}\right)$$
$$+ \frac{1}{60} \cdot \sum_m \left(b_{4m}O_{4m} + c_{4m}\Omega_{4m}\right), \qquad (6)$$

where **S** is the electron spin operator, $b_{nm}$, $c_{nm}$ are the fine structure parameters, $O_{nm}$, $\Omega_{nm}$ are the cosine and sine Stevens spin operators. Measured and calculated orientation behavior of transition positions of this center is shown in Figure 3. Taking into account the magnitude of spin of this center and its occurrence at room temperature without hyperfine structure, it is fair to say that the specified center

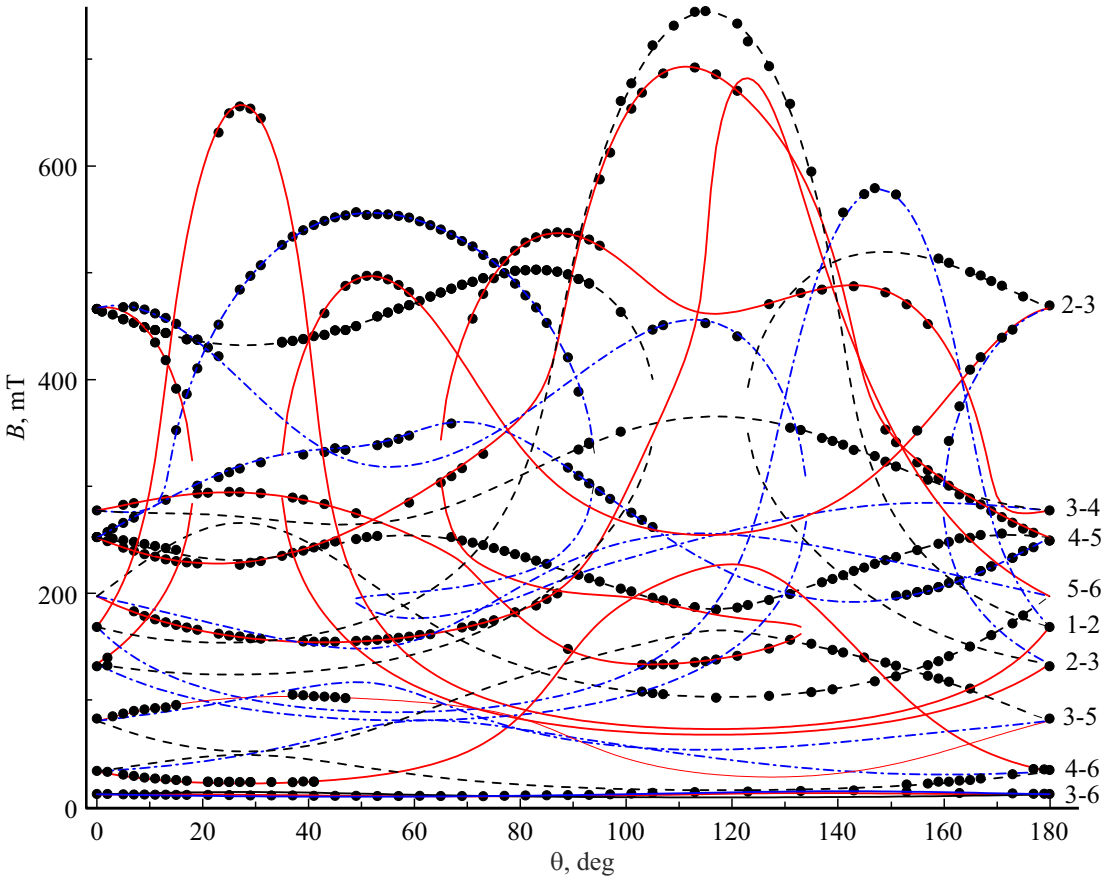


**Figure 3.** Orientation behavior in the $ZX$ plane of transition positions between the aforesaid energy levels (Figure 2, $b$) of three $Fe^{3+}$ centers, points — measurements, curves — calculation using parameters of Table, solid curves — $\varphi = 0°$, dashed curves — $\varphi = 120°$, dash-dotted curves — $\varphi = 240°$.

is $Fe^{3+}$ ion. Since $Fe^{3+}$ impurity ions as well as $Cr^{3+}$ centers in corundum, garnet, chrysoberyl, perovskite, spinel, lanthanum gallate structures take octahedrally coordinated aluminum, titanium or gallium positions, the observed centers are definitely placed in $Al^{3+}$ position with oxygen-fluorine environment and local $\bar{1}(C_i)$ symmetry. Crystal $C_3$ symmetry operation multiplies this position up to three ones. The broad signal width (Figure 2, $a$) prevents a superhyperfine (from $^{19}F$ with nuclear spin $I = 1/2$) structure to be detected.

Fine structure parameters of $Fe^{3+}$ centers obtained by means of minimization of rms deviation of the calculated frequencies from the measured frequencies (44 MHz is the best value), including 431 transition positions of three centers coupled by $C_3$ operation are listed in the Table. The **g**-tensor was considered to be isotropic with a value of 2.00, and the coordinate system used for the calculations is described in the beginning of Section 3.1. Rather high rms deviation is due to wide signal width of $Fe^{3+}$ centers and error in $\theta$ angles, which is certainly most clearly pronounced in the curve segments with large $dB/d\theta$ (Figure 3). The Table also contains the spin Hamiltonian parameters in the principal axes of the second-order tensor determined by means of maximization of $b_{20}$. It can be seen that the SH second-order tensor in the principal axes becomes diagonal, i.e. rhombic. This CS is coupled with the laboratory system

Fine structure parameters of triclinic $Fe^{3+}$ centers in NAPF in the laboratory coordinate system and principal axes of the second-order tensor. Sign of $b_{20}$ was not defined

| Parameters, in MHz | $Z \parallel c$ | In principal axes of the second-order tensor |
|---|---|---|
| $b_{20}$ | 680 | −4280 |
| $b_{21}$ | 9740 | 0 |
| $b_{22}$ | −4300 | 1330 |
| $c_{21}$ | 860 | 0 |
| $c_{22}$ | −360 | 0 |
| $b_{40}$ | 40 | −50 |
| $b_{41}$ | 240 | 200 |
| $b_{42}$ | 40 | 70 |
| $b_{43}$ | 2000 | −570 |
| $b_{44}$ | 340 | −800 |
| $c_{41}$ | −250 | −410 |
| $c_{42}$ | −360 | 70 |
| $c_{43}$ | 280 | −960 |
| $c_{44}$ | −70 | −180 |

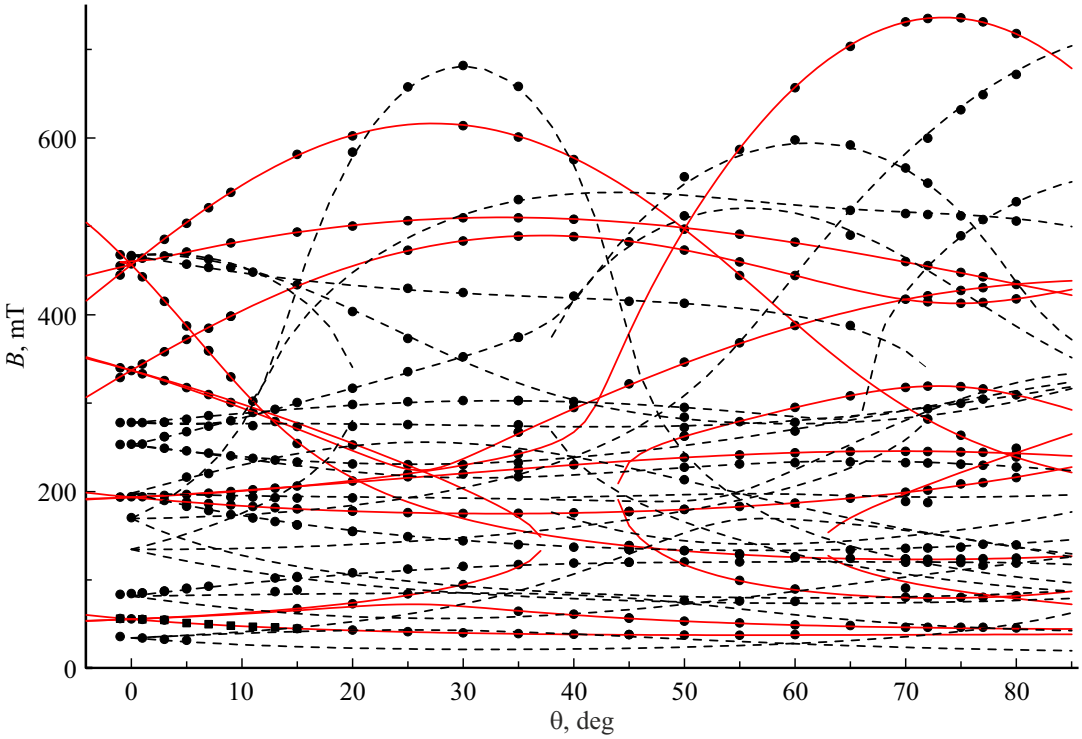


**Figure 4.** Polar angular dependence of $Cr^{3+}$ (solid curves) and $Fe^{3+}$ (dashed curves) center transition positions with magnetic field rotation around the crystallographic $b$ axis.

XYZ by the Euler angles $\alpha_{21} = 197.5°$, $\beta_{21} = 64.4°$ and $\gamma_{21} = 210.6°$ (the first digit in the subscript is the fine structure tensor rank, the second digit is the magnetically nonequivalent center number). The coordinate systems of the other two magnetically nonequivalent centers are obtained by additional 120-degree rotation about the $C_3$ axis of the crystal: $\alpha_{22} = 317.5°$, $\beta_{22} = 64.4°$, $\gamma_{22} = 210.6°$, $\alpha_{23} = 77.5°$, $\beta_{23} = 64.4°$, $\gamma_{23} = 210.6°$.

Figure 3 in [1] shows the angular dependences of transition positions of $Cr^{3+}$ centers when the magnetic field is rotating about the crystallographic $b$ axis, which demonstrate that the spectrum description does not deteriorate as the azimuth angle changes. For the same purpose (spectrum azimuthal dependence testing), Figure 4 shows the calculated and measured orientation behavior of $Fe^{3+}$ and $Cr^{3+}$ center resonance positions at $\varphi = -12.5°$ of the laboratory CS. $V^{4+}$ center transition positions are not shown for the sake of simplicity.

It was already reported in [1] that it is not possible to associate unambiguously the given local system with a certain octahedron containing $Cr^{3+}$ ion, i.e. to determine which paramagnetic center of the crystalline structure governs the given spectrum with the principal axes associated with it. And, therefore, it is not possible to identify the strain direction of the octahedron containing $Fe^{3+}$ ion or $Cr^{3+}$ ion.

It was observed that in the laboratory coordinate system of $Fe^{3+}$ centers (see the Table) a high value of $b_{43}$ is observed among other $b_{4m}$ and $c_{4m}$ parameters, which may imply that the $z$ axis of this CS is close to the pseudotrigonal axis of the distorted octahedron with the iron ion. When they coincide approximately a minimum of the sum of squares of $b_{41}$, $b_{42}$, $b_{44}$, $c_{41}$, $c_{42}$ and $c_{44}$ [17,18] can be expected.

Actually, the sum of squares of fourth-order parameters ($Q_{43}$), not including $b_{43}$ and $b_{40}$, in the coordinate system defined by the Euler angles $\alpha_1(43) = 319.3°$, $\beta_1(43) = 17.2°$, $\gamma_1(43) = 47.8°$ (relative to the laboratory CS, $\beta$ is the angle between the $Z$ and $z_1$ axes) shows the following minimum $Q_{43} \sim 8 \cdot 10^4\,\mathrm{MHz}^2$ and SH parameters (in MHz): $b_{44} = 79.3$, $b_{43} = 2428.2$, $b_{42} = 235.9$, $b_{41} = 151.9$, $b_{40} = 86.0$, $c_{41} = -31.2$, $c_{42} = -11.3$, $c_{43} = 0$, $c_{44} = 60.0$. It can be seen that $b_{43}/b_{40} = 28.2$ is close to $20 \cdot \sqrt{2}$ which is typical of the cubic center with $z \parallel C_3$ [19].

There are other minimum values of sum $Q_{43}$ equal to $\sim 8 \cdot 10^4\,\mathrm{MHz}^2$ whose $z_i(43)$ axes make angles with $z_1(43)\{\alpha_1(43), \beta_1(43), \gamma_1(43)\}$ which are close to (difference $\leq 4°$) the canonical angles between the trigonal axes of the regular octahedron (70.6° and 109.4°). The ratio of $b_{43}/b_{40}$ in this minima varies within the range of 22–31, i.e. they are almost equivalent. The $z_i(43)$ axes of the specified minima may be assumed as approximately corresponding to the trigonal direction of the distorted fluorine-oxygen octahedron $C$ in Figure 5, and the difference in kind of ligands is ignored in this case. It can be seen that the detected $z_i(43)$ directions in another two octahedra ($A$ and $B$) are far from pseudotrigonal axes.

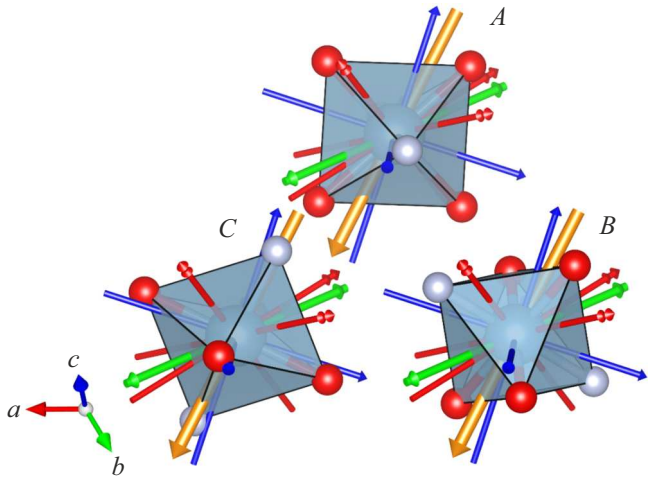


**Figure 5.** Fluorine-oxygen octahedra in NAPF structure transferring into each other with rotation at $\pm 120^\circ$ around the $c$ axis. Red thin double-headed arrows are directions corresponding to minimum $Q_{43}$; blue thin single-headed arrow are directions corresponding to minimum $Q_{44}$; yellow thick arrows are the principal second-order axes of $Fe^{3+}$; green middle-thickness single-headed arrows are principal second-order axes $Cr^{3+}$.

The sum of squares of the fourth-order parameters ($Q_{44}$) of $Fe^{3+}$ centers that does not include $b_{44}$ and $b_{40}$ demonstrates one minimum with $Q_{44} \sim 1.4 \cdot 10^4$ MHz$^2$ and $b_{44}/b_{40} \sim \pm 10$ $\{\alpha_1(44) = 200.1^\circ,\ \beta_1(44) = 47.6^\circ,\ \gamma_1(44) = 161.1^\circ\}$. Angles between $z_1(44)$ and $z_i(43)$ are within $56-59^\circ$ which is somehow higher than angle $54.7^\circ$ corresponding to the minimum angle between the tetragonal and trigonal axes of the regular octahedron.

It is reasonable to associate the principal axis of the specified minimum spaced away from the Al-F axis at $\sim 8^\circ$ in the octahedron with the only pseudotetragonal fluorine-fluorine direction (Figure 5), it shall be also noted that for the ion in the tetragonally distorted octahedron, the ration $b_{44}/b_{40}$ may differ from $\pm 5$ [19], which is only implemented for the cubic symmetry. In addition, there are minima with $Q_{44} \sim 8.2 \cdot 10^4$ MHz$^2$ and $b_{44}/b_{40} \sim 3.7$ whose $z_i(44)$ axes, according to their Euler angles, are approximately orthogonal to the $z_1(44)$ axis and close to the directions towards oxygen ions (Figure 5). Thus, it is fair to say that the fourth-order fine structure tensor of $Fe^{3+}$ centers in NAPF is quasitetragonal and its axes adequately reflect the fluorine-oxygen octahedron structure elements. The second-order tensor is rhombic and its principal axis is deviated from the specified quasitetragonal axis at $\sim 17^\circ$ (see Figure 5) due to its stronger dependence on the octahedron distortions.

It is suggested that there is low dependence between the fluorine-oxygen octahedron distortion behavior and the impurity ion within the octahedron, and then the principal axes directions of the second-order tensors of $Fe^{3+}$ and $Cr^{3+}$ centers shall be close to each other. However, Figure 5 shows that the principal axes directions of the chromium center fine structure in all fluorine-oxygen octahedra are close to quasitrigonal axes, rather than to the fluorine-fluorine direction of the octahedron. Hence, it can be concluded that various impurity defects cause significantly different distortions in the nearest environment.

## 4. Conclusion

In $Na_5AlF_2(PO_4)_2$ : Cr crystal, occasional $V^{4+}$ ($S = 1/2$) and $Fe^{3+}$ ($S = 5/2$) impurity centers were detected and investigated. Measurement of the orientation behavior of EPR positions for the transitions of three $V^{4+}$ centers associated with $C_3$ operation with the crystal allowed to determine SH parameters of these centers both in the laboratory and principal coordinate systems, where the hyperfine interaction tensor becomes rhombic. Taking into account the principal axis orientation of $V^{4+}$, it was concluded that the phosphorus position is substituted by vanadium. The comparison of local coordinate system axes orientation of the second-order and fourth-order fine structure tensors of $Fe^{3+}$ centers with the distorted octahedron showed that the principal axes are close to the F-F direction of the fluorine-oxygen octahedron surrounding the iron ion.

### Acknowledgments

The authors would like to express gratitude to B.K. Sevatianov and V.F. Tarasov for provision of specimens, to G.S. Shakurov for his interest in the research, and to V.A. Shustov for crystal orientation in the X-ray diffractometer.

### Funding

The study was performed with the financial aid provided by the Ministry of Science and Higher Education of the Russian Federation, theme No. FEUZ-2023-0017 using the equipment provided by Ural Common Use Center „Modern Nanotechnologies“ Ural Federal University (Reg. No. 2968) supported by the Ministry of Science and Higher Education of the Russian Federation (project 075-15-2021-677).

### Conflict of interest

The authors declare that they have no conflict of interest.

## References

[1] V.A. Vazhenin, A.P. Potapov, A.V. Fokin, M.Yu. Artemov. FTT **63**, *11*, 1915 (2021) (in Russian).
[2] J. Arlt, M. Jansen, H. Klassen, G. Schimmel, G. Heymer. Z. Anorg. Allg. Chem. **547**, 179 (1987).
[3] D.M. Poojary, A. Clearfield, V.A. Timofeeva, S.E. Sigaryov. Solid State Ionics **73**, 75 (1994).
[4] A.K. Ivanov-Shits, S.E. Sigariov, V.A. Timofeeva. FTT **32**, *2*, 624 (1990) (in Russian).

[5] A.K. Ivanov-Shits, S.E. Sigaryov. Solid State Ionics **40/41**, 76 (1990).
[6] V.A. Timofeeva, Rost kristallov iz rastvorov-rasplavov Nauka, M., (1978). 267 p. (in Russian).
[7] John Lambe, Chihiro Kikuchi. Phys. Rev. **118**, *1*, 71 (1960).
[8] H.J. Gerritsen, H.R. Lewis. Phys. Rev. **119**, *3*, 1010 (1960).
[9] Chihiro Kikuchi, Inan Chen, William From, Paul B. Dorain. J. Chem. Phys. **42**, *1*, 181 (1965).
[10] I.N. Geifman, P.G. Nagorny, A.N. Usov, Fam za Ngy. FTT **33**, *9*, 2716 (1991) (in Russian).
[11] I.N. Geifman, P.G. Nagorny, M.V. Rotenfeld. FTT **36**, *12*, 3550 (1994) (in Russian).
[12] I.N. Geifman, I.S. Golovina, P.G. Nagorny. FTT **40**, *3*, 534 (1998) (in Russian).
[13] Dzh. Verts, J. Bolton. Teoriya i prakticheskie prilozheniya metoda EPR. Mir, M. (1975). 547 p. (in Russian).
[14] A. Abragam, B. Blini. Elektronnyj paramagnitnyj rezonans perekhodnykh ionov. Mir, M. (1973). 347 p. (in Russian).
[15] V.I. Pet'kov, M.V. Sukhanov, A.S. Shipilov, V.S. Kurazhkovskaya, E.Yu. Borovikova, N.V. Sakharov, M.M. Ermilova, N.V. Orekhova. Zhurn. neorgan. khimii **58**, *1139*, 2013 (2012) (in Russian).
[16] S.A. Altshuler, B.M. Kozyrev. Elektronnyi paramagnitnyi rezonans soedineniy elementov promezhutochnykh grupp. Nauka, M., (1972). P. 121. (in Russian).
[17] R.L. White, G.F. Herrmann, J.W. Carson, M. Mandel. Phys. Rev. **136**, *1A*, 231 (1964).
[18] N.M. Nizamutdinov, N.M. Khasanova, G.R. Bulka, V.M. Vinokurov, I.S. Rez, V.M. Garmash, N.I. Pavlova. Kristallografiya **32**, *695*, 1987 (1990) (in Russian).
[19] M.L. Meilman, M.I. Samoilovich. Vvedeniye v spektroskopiyu EPR aktivirovannykh monokristallov. Atomizdat, M. (1977). P. 109. (in Russian).

*Translated by Ego Translating*